Dynamics of the Wind-Driven Sea Level Variation around Antarctica

KAZUYA KUSAHARA*

Graduate School of Environmental Earth Science, and Institute of Low Temperature Science, Hokkaido University, Sapporo, Japan

KAY I. OHSHIMA

Institute of Low Temperature Science, Hokkaido University, Sapporo, Japan

(Manuscript received 18 January 2008, in final form 19 August 2008)

ABSTRACT

Coastal sea level variation around Antarctica is characterized by a coherent (circumpolarly in-phase) fluctuation, correlated with the Antarctic Oscillation (AAO). This study addresses the dynamics of the wind-driven sea level variation around Antarctica. A realistic barotropic numerical model reproduced well the observed sea level around Antarctica. From numerical model experiments, the authors demonstrate that the forcing responsible for the coastal sea level is the wind stress at the coastal boundary. Both the dominant coherent signal and westward propagating signals are identified in the model, and these signals are trapped over the shelf and slope around Antarctica. As a mechanism of these trapped signals, the authors consider analytical solutions of the oceanic response to alongshore wind stress over the shelf and slope in the circumpolar domain. In these solutions, besides the shelf wave mode, a wavenumber-zero mode appears and characterizes the coastal dynamics around Antarctica. At periods from 10 to 200 days, the coherent sea level can be explained quantitatively by the solution of this wavenumber-zero mode with a 5–10-day damping time scale. The spectral peaks of the westward propagating signals can be explained by the resonance of the shelf wave mode. The wavenumber-zero mode can respond to the wavenumber-zero forcing at any frequency and the degree of response increases with decreasing frequency. In addition, the wavenumber-zero component of wind stress, corresponding to the AAO variation, is a dominant forcing. Therefore, the coherent sea level variation around Antarctica is preferably generated and becomes a dominant feature in the circumpolar domain, particularly at lower frequencies.

1. Introduction

The Southern Ocean, including the Antarctic Ocean, has no east–west boundary and directly connects three major oceans: the Pacific, Atlantic, and Indian Oceans. Wind stress in the Southern Ocean is the strongest in the world, both in its mean and variability. Therefore, wind-driven currents in this ocean, such as the eastward-flowing Antarctic Circumpolar Current (ACC) and the westward-flowing Antarctic Coastal Current, also have large variability, interacting with bottom topography.

From both observational and numerical model studies, it is well known that the response of the Southern Ocean is highly barotropic at periods shorter than 1 yr (Peterson 1988; Chao and Fu 1995; Fu and Davidson 1995; Vivier et al. 2005). To estimate the ACC transport variability, sea level or sea level difference from satellite altimetry and bottom pressure data have often been used (Peterson 1988; Meredith et al. 1996, 2004; Woodworth et al. 1996, 2006; Gille et al. 2001; Meredith and Hughes 2004). Focusing on sea level variation, except for tidal forcing, three major causes can be considered. First, thermal expansion, including the ice melting/freezing process, mainly contributes to the annual variation (Vivier et al. 2005). Second, surface atmospheric pressure variations drive westward propagating Kelvin waves around Antarctica at periods shorter than 2 days (Ponte 1993; Hirose et al. 2001; Ponte and Hirose 2004). Last, wind stress drives the oceanic variability, including sea level, and its barotropic response is a dominant

* Current affiliation: Center for Climate System Research, University of Tokyo, Chiba, Japan.

Corresponding author address: Kazuya Kusahara, Center for Climate System Research, University of Tokyo, 5-1-5, Kashiwanoha, Kashiwa-shi, Chiba, 277-8568, Japan.
E-mail: kusahara@ccsr.u-tokyo.ac.jp

DOI: 10.1175/2008JPO3982.1

feature south of 50°S over a broad range of periods from a few days to one year (Vivier et al. 2005).

In the Southern Ocean, the variation of wind stress affects sea level over a broad range of periods, from a few days to century time scales. The dominant atmospheric mode in the Southern Hemisphere is the Antarctic Oscillation [AAO; also known as the southern annular mode (SAM)] (Thompson and Wallace 2000), which is characterized by an annular structure and relates strongly to the variation of wind stress. Based on a climate model, Hall and Visbeck (2002) investigated the response of ocean circulation to the AAO variations at periods from a few days to century time scales. In the positive phase of the AAO index, an intensification of eastward wind stress occurs, and thus an anomalous northward Ekman transport is generated at the ocean surface. Subsequently, a fall of coastal sea level (a rise of the internal surface) and an intensification of the eastward currents occurs.

Since the Antarctic coastal ocean is located in a seasonal sea ice zone, continuous records of in situ ocean measurements (such as moorings) and satellite measurements (such as altimetry) are difficult to obtain. Taking account of these circumstances, sea level observation at some coastal stations around Antarctica is the only observation that has monitored long-term oceanic conditions continuously, resulting in a very valuable dataset in the Antarctic oceanic region. Aoki (2002) and Hughes et al. (2003) analyzed the coastal sea level variations around Antarctica and demonstrated that the variation at periods shorter than 1 yr is characterized by a circumpolarly in-phase (coherent) fluctuation and is significantly anticorrelated with the AAO index. Such coherent fluctuation had already been suggested in some studies (Woodworth et al. 1996; Hughes et al. 1999) in which the coherent signal was identified in their numerical models with the comparison to the regionally limited observation. We will use ''coherent'' to mean ''circumpolarly in-phase'' hereinafter, following Aoki (2002) and Hughes et al. (2003). The observed negligible time lag between the coherent sea level and the AAO index implies that a strong damping mechanism is necessary for the dynamics. Using a barotropic numerical model, Vivier et al. (2005) showed that this coherent variation is confined near Antarctica and is responsible for most of the barotropic circumpolar transport.

The coastal sea level around Antarctica is known to be a proxy of the ACC variation. For the ACC variation, Wearn and Baker (1980) discussed the response to the circumpolar-averaged wind stress on the basis of a simple analytical model. Using an unstratified OGCM, Weijer and Gille (2005) showed that the ACC transport response to the zonally averaged wind stress becomes larger at lower frequencies (i.e., the spectrum is redden). They also showed that topographic form drag can be the damping mechanism for the ACC transport and estimated its time scale as the order of 3 days.

On the other hand, the coastal current variation at subinertial frequency, which is closely related to the coastal sea level variation, is mainly determined by local coastal dynamics over the shelf and slope. From current meter records over the shelf and slope in the Weddell Sea (Middleton et al. 1982; Fahrbach et al. 1992) and Lützow–Holm Bay (Ohshima et al. 2000), the current variability at subinertial frequency is mostly governed by the shelf waves driven by the alongshore wind stress.

For the dynamics of sea level variation around Antarctica, although it has been proposed that anomalous north–southward Ekman transport corresponding to the AAO variation is qualitatively important, the mechanism has not been well understood. The purpose of this study is to clarify quantitatively the dynamics of the sea level around Antarctica. Based on the result of the observations and numerical model, we consider the analytical solutions of coastal response to the wind forcing in the circumpolar domain and discuss the mechanism of the coherent variation. In particular, we focus on why the coherent sea level variation around Antarctica is by far the dominant feature.

2. Data and barotropic shallow-water model

Hourly sea level data are available from Syowa, Mawson, Davis, Casey, and Vernadsky (formerly Faraday) Stations (see Fig. 1 for locations). Six years of data were used from Syowa, Mawson, Davis, and Vernadsky (1994–99), and four years from Casey (1996–99). These hourly sea level data at Syowa and the other four stations were obtained from the Japan Oceanographic Data Center and British Oceanographic Data Centre, respectively. These data were corrected to give subsurface pressure (sea level corrected for the inverse barometer effect) by means of hourly air pressure data calculated with cubic splines from observed sea level air pressure data. In the remainder of this paper, we refer to the subsurface pressure as ''sea level.'' Air sea level pressure data at the five stations were obtained from the British Antarctic Survey. Since the time series of sea level pressure of 40-yr European Centre for Medium-Range Weather Forecasts Re-Analysis (ERA-40) data with $1.125° \times 1.125°$ resolution agrees well with those of the station observations, ERA-40 values were used for temporal lack of observed data. Ten components of tides (M_2, S_2, K_1, O_1, N_2, P_1, K_2, Q_1, Mm, Mf) were

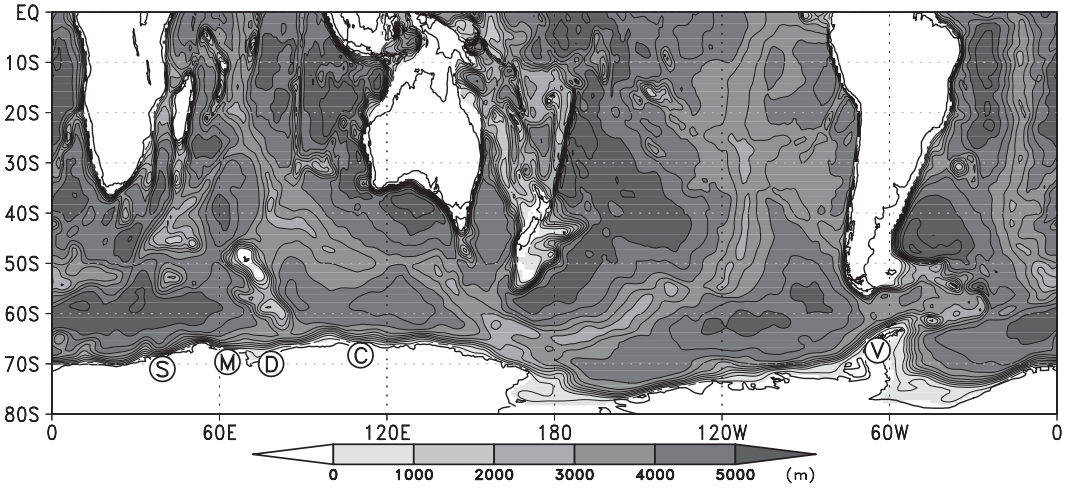

FIG. 1. Domain and bottom topography of the barotropic shallow-water model with locations of tide gauges: Contour interval is 500 m. Labels S, M, D, C, and V indicate Syowa, Mawson, Davis, Casey, and Vernadsky Stations, respectively.

estimated and removed using harmonic analysis. After such processing, daily means were used in the following analyses. The daily AAO index was obtained from the National Oceanic and Atmospheric Administration/National Weather Service/Climate Prediction Center (NOAA/NWS/CPC).

We used a barotropic shallow-water model in spherical coordinates, with a hydrostatic approximation, and a horizontal resolution of 0.5° and 1° in the meridional and zonal direction, respectively. The model domain surrounds the Antarctic continent and extends to an artificial boundary at the equator (Fig. 1). A nonslip boundary condition was used for lateral boundaries. To model a spindown effect by the bottom Ekman layer, bottom friction is parameterized in a linear form as $-r\mathbf{u}/H$, with constant coefficient $r = 5.0 \times 10^{-4}$ m s^{-1} (Chapman et al. 1986), where H is ocean depth and $\mathbf{u}$ is depth-averaged horizontal velocity. Horizontal viscosity is parameterized in a Laplacian form, and its coefficient is set to a constant value of 5.0×10^3 m^2 s^{-1}. A buffer region was placed in latitudes from 30°S to the equator, where the horizontal viscosity gradually increases to 20 times its interior value toward the northern boundary.

The wind stress was calculated from 6-hourly ERA-40 wind data at 10-m height above the sea surface using the bulk formula (Trenberth et al. 1990). The existence of sea ice was ignored in the model. Bottom depth data were derived from 5′ gridded elevations/bathymetry for the world (ETOPO5) (National Geophysical Data Center 1988), and the model depth was smoothed by averaging the depth at each grid point and its four adjacent grid points. In the shelf region adjacent to the Antarctic continent, grid points with depths shallower than 100 m were set as land points. In regions away from Antarctica, grid points with depths shallower than 500 m were set as land points to suppress numerical instability. Figure 1 shows the bottom topography of the model.

To focus on the time variation, the barotropic model was driven by the anomaly from a 1-yr running mean of wind stress. The model was run from 1993 to 1999. For the following analyses, daily averaged values from 1994 to 1999 were used.

3. Numerical model results

In this section, we show the results of the barotropic numerical model forced by a realistic wind stress anomaly. The model reproduced well the observed sea level variation at the stations around Antarctica in the time series (Fig. 2a). For quantitative comparison in the frequency domain, spectral analyses were performed for the observed and modeled sea levels (Figs. 2b–d). Results of Mawson and Vernadsky Stations are presented as representative East and West Antarctica cases, respectively. For smoothing the spectra in the frequency domain, a box filter with band averaging over 9 (41) adjacent frequencies was performed below (above) 0.05 cpd. At periods shorter than 200 days, the barotropic model reproduces the observed sea level well, from the similar profile of the power spectra (Fig. 2b), significant coherence (Fig. 2c), and the agreement in phases (Fig. 2d) between the observed and modeled sea levels. For the other stations (Syowa, Davis, Casey), similar results are obtained.

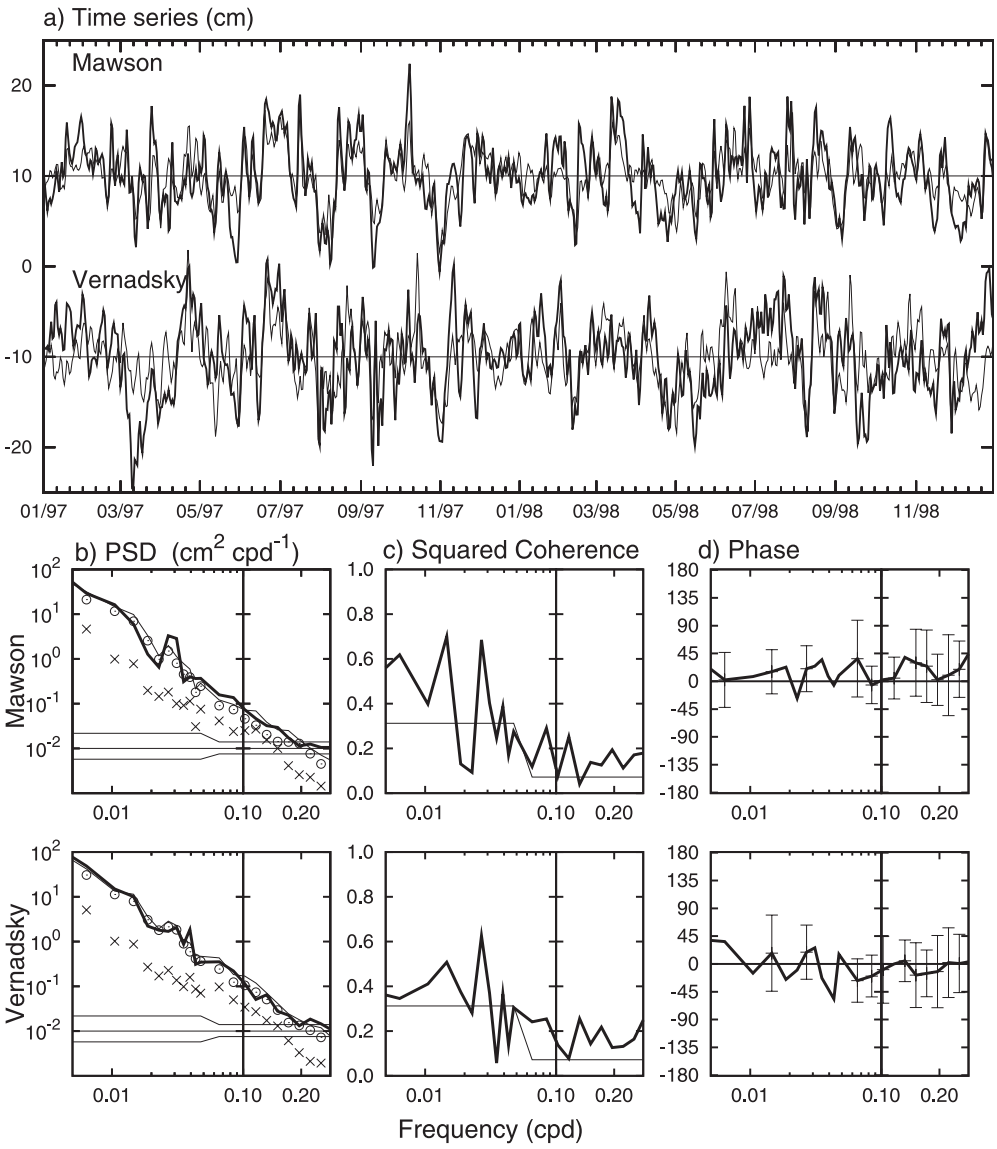

FIG. 2. (a) Time series of the sea level from the observation (thick lines) and the model (thin lines) at Mawson (with an offset of + 10 cm) and Vernadsky (with an offset of −10 cm) Stations for 1997–98. A 3–200-day bandpass filter was applied to these time series. (b)–(d) Results of spectral analyses for sea levels at (middle) Mawson and (bottom) Vernadsky Stations. (b) Power spectra of the observed sea level (thick lines) and modeled sea level (thin lines: experiment driven by the original wind stress; open circles: coastal experiment; crosses: offshore experiment). (c) Squared coherence of the cross-spectra between the observed and modeled sea levels. (d) Phase of the cross-spectra. The horizontal axis in all panels indicates frequency (unit: cpd), where a log scale is used for the frequency (periods) from 0.005 cpd (200 days) to 0.1 cpd (10 days) and a linear scale for the frequency (periods) 0.1 cpd (10 days) to 0.25 cpd (4 days). In (d) a positive value indicates that the observation leads the model. The 95% confidence interval or level is also shown in each panel.

a. Forcing responsible for the coastal sea level

To identify which part of the wind stress is responsible for the coastal sea level variation around Antarctica, two numerical model experiments, forced solely by coastal wind stress (coastal experiment) and solely by offshore wind stress (offshore experiment), were performed. To make the wind stress field for the two numerical experiments, we use the following weight function:

$$w(H) = \begin{cases} 0.5 \times [1 - \tanh(\frac{H-4500}{500})] & \text{south of } 60^\circ\text{S} \\ 0 & \text{north of } 60^\circ\text{S}, \end{cases}$$

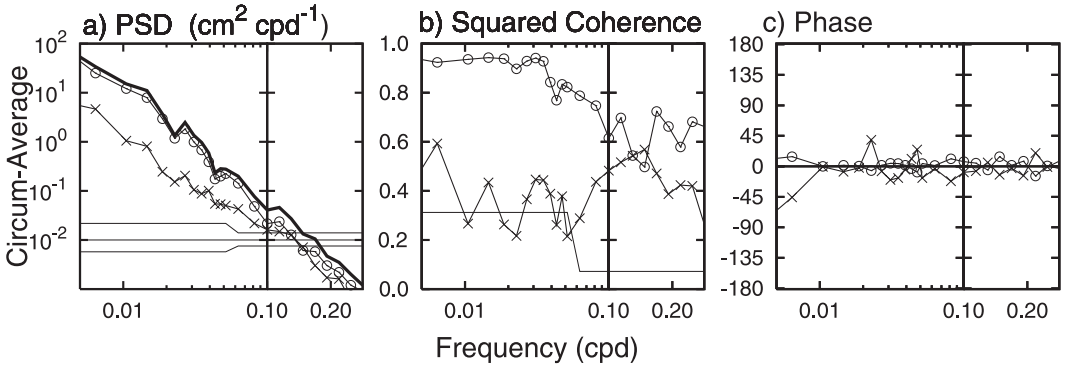

FIG. 3. Results of spectral analyses for circum-averaged coastal sea level in the numerical model. Thick and thin line indicate sea level driven by the original wind stress and modified wind stress (open circles: coastal experiment; crosses: offshore experiment), respectively. (a) Power spectra for the three experiments. (b) Squared coherence of the cross-spectra between the original experiment and modified wind stress experiments. (c) Phase of the cross-spectra. The horizontal axis in all panels indicates frequency (unit: cpd), where a log scale is used for the frequency (periods) from 0.005 cpd (200 days) to 0.1 cpd (10 days) and a linear scale for the frequency (periods) 0.1 cpd (10 days) to 0.25 cpd (4 days). The 95% confidence interval or level is also shown in (a) and (b).

where H is the water depth (in meters). The wind stress field for the coastal experiment is obtained by multiplying the original wind stress field and the weight function. This wind field is almost the same as the original wind field in the coastal regions shallower than 4000 m. The wind stress field for the offshore experiment is obtained by subtracting the above coastal wind stress field from the original wind stress field.

The power spectra of the coastal sea level at the two stations and of the circum-averaged one for the two experiments are shown in Figs. 2b and 3a, respectively. The power spectra for the coastal experiment are almost identical to those for the experiment driven by the original wind stress, but those for the offshore experiment have much smaller amplitude, by one order of magnitude. For the circum-averaged sea level at periods longer than 10 days, a significant high coherence and agreement in phase between original and coastal experiments can be found (Figs. 3b,c). These results indicate that the coastal sea level variation around Antarctica is driven by the coastal wind stress and not by the offshore wind stress. In the following, the results using the original wind stress are shown, while the coastal experiment shows almost the same results.

b. *Characteristics in the frequency–wavenumber domain*

The alongshore component of wind stress can be a main driving force of coastal ocean variability at periods longer than a few days (Gill and Schumann 1974; Csanady 1982). Thus, we performed space–time (frequency–wavenumber domain) spectral analysis (Hayashi 1971) both for the alongshore wind stress averaged to 500 km from the coast and the coastal sea level around Antarctica in the model, where the spatial domain is taken as the circumpolar coastal grid points around Antarctica (the total distance is about 15 700 km) and the time domain is taken as the period from 1994 to 1999. The circumpolar coastal grid points in the model are defined as the nearest grid points from the Antarctic continent. Hence, some grid points are aligned in the meridional direction, as seen in the western part of the Ross and Weddell Seas. A direction of alongshore wind stress at each grid point is defined as a direction parallel to the large-scale bottom topography contours, which were calculated from the smoothed depth data (ETOPO5) over a 12.375° × 12.375° grid in the longitudinal and latitudinal direction.

In the frequency–wavenumber domain, signals can be expressed by the superposition of the wavenumber-zero, eastward and westward propagating components. A superposition of eastward and westward propagating waves with the same amplitude makes a standing wave for a certain frequency. Therefore, the signals can be also expressed by the superposition of the wavenumber-zero component, a standing wave, and a purely (eastward or westward) propagating wave for a certain frequency. The coherent fluctuations are divided into spatially uniform and nonuniform components, which correspond to the wavenumber-zero and standing wave components, respectively. The nonuniform components (standing wave) come from the irregular coastline and variable water depth in the alongshore direction. From our calculation, the amplitude of the standing wave is found to be smaller by one order of magnitude than that of wavenumber zero for both wind stress and sea level. Thus, the components of the

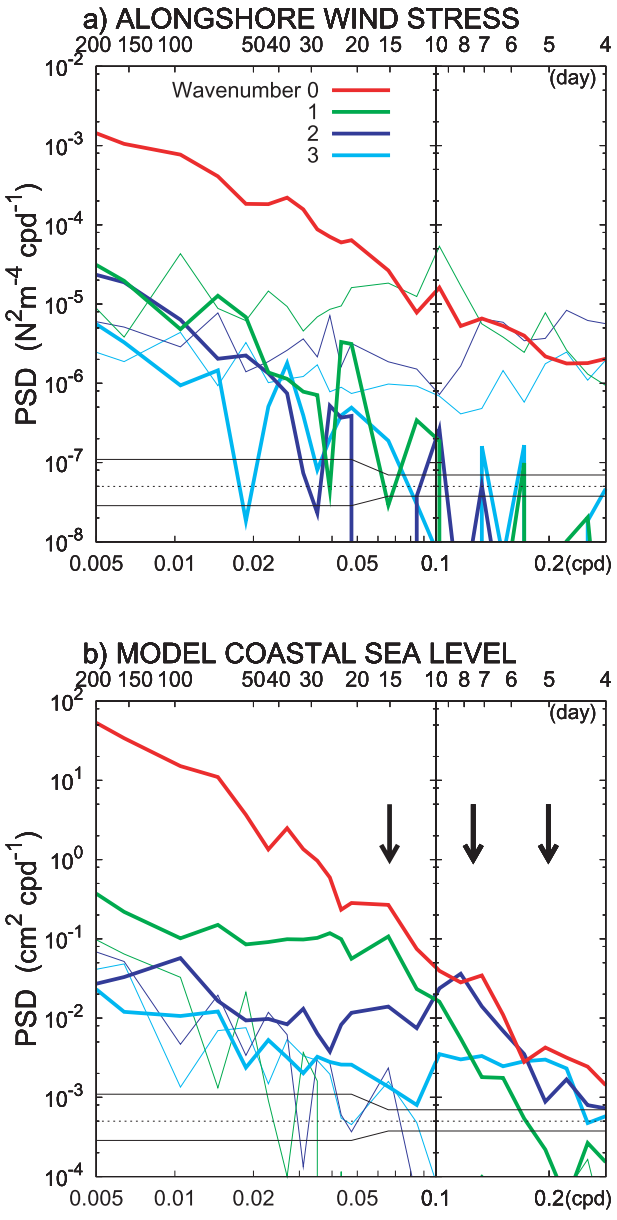

FIG. 4. Power spectra from space–time spectral analyses for (a) alongshore wind stress and (b) coastal sea level in the model. Thick and thin lines indicate westward and eastward components, respectively. After removal of the standing waves (see the text for the detail), band averaging is performed, causing nonzero amplitudes of both components for each frequency. The lower and upper horizontal axes indicate frequency (unit: cpd) and period (unit: day), respectively. In the horizontal axes, log and linear scales are used below and above 0.1 cpd, respectively. The 95% confidence interval is also shown in each panel. In (b) arrows indicate the resonant periods derived from the analytical solution.

standing wave will not be examined in detail in this study. In the following analyses, the components of the standing waves were removed to extract purely propagating components.

From the power spectrum of the alongshore wind stress at each wavenumber (Fig. 4a), the amplitude of wavenumber zero is the largest component at periods longer than a few days, particularly by far the dominant one at periods longer than 20 days. At periods shorter than 20 days, the amplitude of eastward propagating signals caused by atmospheric synoptic-scale disturbances is nearly comparable to that of wavenumber zero. On the other hand, the amplitude of westward propagating signals of the wind stress is much smaller at any frequency. From the power spectra of the coastal sea level in the model (Fig. 4b), the amplitude of wavenumber zero is the largest component, as in the case of the alongshore wind stress. The spectral slope of the wavenumber-zero sea level is significantly steeper than that of the wavenumber-zero forcing (Fig. 4). This suggests a transfer function that enhances the oceanic response at low frequencies compared to high frequencies. It is also noted that peaklike features can be found in the westward propagating signals at a period around 15 days for wavenumber one and 7–8 days for wavenumber two.

c. *Coherent mode*

From the observational results, sea level variations at periods longer than 10 days are characterized by the coherent variation along the coast (Aoki 2002; Hughes et al. 2003). Empirical orthogonal function (EOF) analysis was applied to the observed sea level at the five coastal stations and to the model results at the coastal grid points (391 points) to extract the dominant variability. To remove high frequency signals at periods shorter than 10 days and the annual signal, a bandpass filter that passes the signal at periods from 10 to 200 days was applied before EOF analysis. In this study, the bandpass filter was designed by using Fourier and inverse Fourier transforms. In both observational and model results, the coherent sea level variations around Antarctica are found as a leading mode, which accounts for 75.3% and 76.9% of the total variance, respectively. Estimating the significance of each leading mode by the Monte Carlo method (Overland and Preisendorfer 1982), both contributions of the leading mode are statistically significant above 99%. To obtain the time series of the representative sea level variations of the leading mode in units of sea level (cm), the mean amplitude (eigenvector) of the five stations and that of the model's coastal grid points were multiplied by the principal component. Figure 5 shows the time series of sea level from observational (red) and model (green) results. These are very similar to each other and the correlation between the two is very high (0.82).

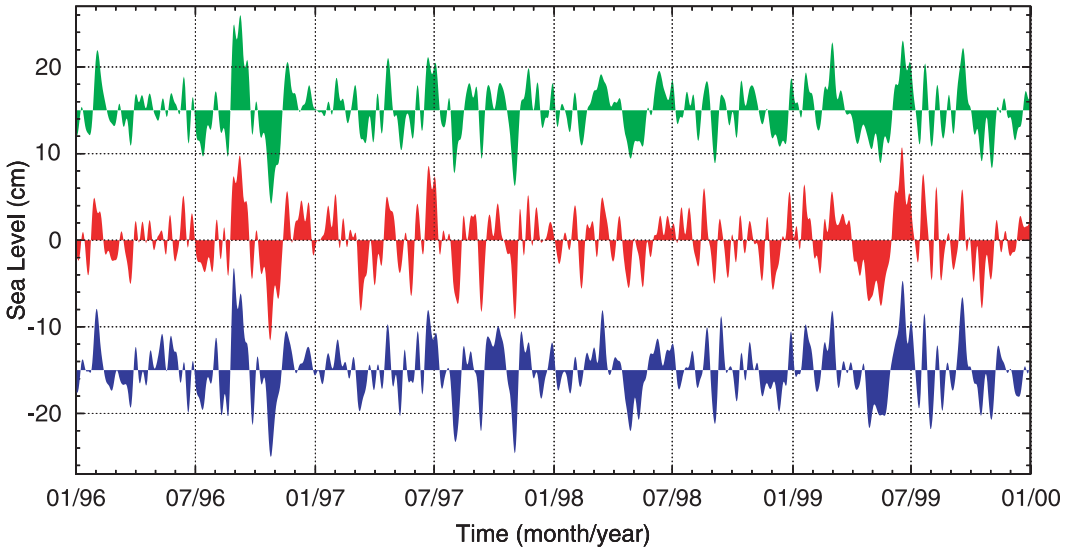

FIG. 5. Time series of the sea level from the observation, model, and analytical solution for 1996–99. The leading modes of the observed and modeled (with an offset of + 15 cm) sea levels are shown in red and green, respectively. The analytical solution with a 5-day damping time scale is shown in blue with an offset of −15 cm.

To examine the spatial feature of the coherent sea level variation in the model, the correlation and regression coefficients between the leading mode and sea level at each grid point in the model were calculated (Fig. 6). Before calculating these coefficients, a 10–200-day bandpass filter was applied to the time series for each model grid point. The high positive correlations (above 0.6) are found over the shelf and slope all around Antarctica (Fig. 6a). The high positive regression coefficients are also found over the shelf and slope all around Antarctica and decrease gradually with depth (Fig. 6b), indicating that the coherent variations have larger amplitude closer to the coast and its amplitude decreases with depth. In brief, the coherent sea level variation around Antarctica is strongly trapped over the shelf and slope. Almost the same result is obtained even using the leading mode of the observed sea level, instead of that of the model (not shown).

d. Westward propagating mode: Wavenumbers 1–3

To understand the characteristics of the westward propagating signals in the model at periods shorter than 20 days, complex empirical orthogonal function (CEOF) analysis (Barnett 1983; Horel 1984) was applied to the coastal sea level variation at the grid points located within a distance of 300 km from the coast. A 3–20-day bandpass filter was applied to the time series of coastal sea level variation in the model before CEOF analysis. Figure 7 shows the spatial distributions of the amplitude (the upper panel) and the phase at the nearest coastal points (the lower panel) for the first four modes in CEOF analysis. The contributions of the first four modes are 47.3%, 15.4%, 9.4%, and 6.5%. These account for about 80% of the total sea level variance in this range of frequencies. For all four modes, the amplitude is larger close to the coast, indicating that the sea level variations are trapped over the shelf and slope. The leading mode of CEOF appears to correspond to the coherent mode. Smaller contribution of the first CEOF than that of the first EOF in the section 3c comes from the difference of the periods (3–20 days for the CEOF, 10–200 days for the EOF). The second, third, and fourth modes have the feature of westward propagation at wavenumber 1, 2, and 3, respectively. These results are consistent with those of the space–time spectral analyses (Fig. 4b). As well as the coherent mode examined in the previous subsection, these westward propagating signals are also trapped over the shelf and slope.

4. Analytical solution of coastal response to the wind forcing in the circumpolar domain

The analyses in the previous section have revealed that the coastal sea level variations around Antarctica are strongly trapped over the shelf and slope. To understand the sea level variations at wavenumbers from 0 to 3 trapped over the shelf and slope all around Antarctica, we consider analytical solutions of the oceanic response to alongshore wind stress over the shelf and slope in the circumpolar domain.

For discussing the coherent mode, we use an analytical solution to the alongshore uniform forcing in an infinite domain. This solution is used for the wavenumber-zero mode in the circumpolar domain. On the other hand,

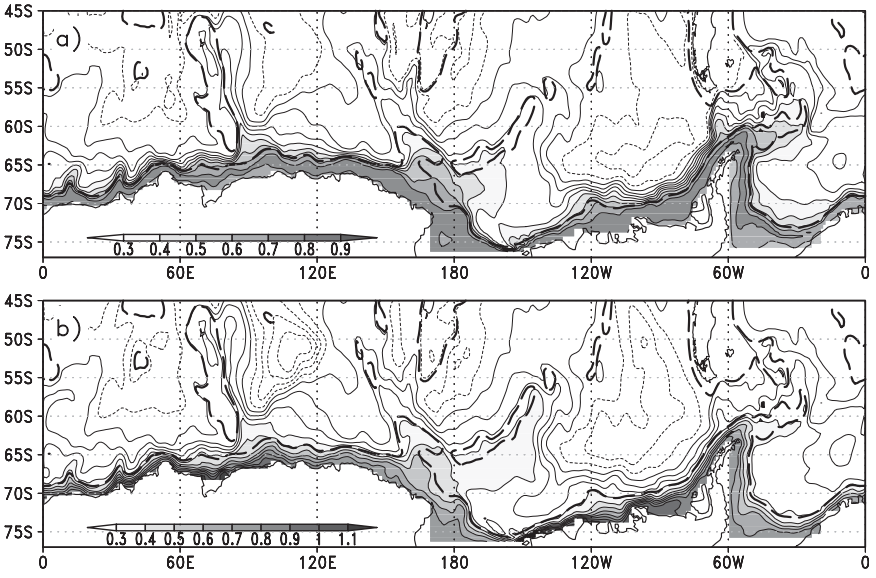

FIG. 6. Maps of (a) correlation and (b) regression coefficient of sea level with the leading mode of the coastal sea level for periods from 10 to 200 days in the model: Contour interval is 0.1 in both panels. The dotted lines indicate negative values. The 3000-m depth contours are denoted by thick dashed lines.

for the propagating mode we use an analytical solution of the barotropic shelf waves (Gill and Schumann 1974), where the horizontal wavenumber (k) takes only quantized integer values because of a cyclic boundary condition in the circumpolar domain ($k = \pm 1, \pm 2, \pm 3, \ldots$).

For simplicity, we assume a straight coastline with water depth H varying only in the cross-shelf direction, and ignore the earth's curvature. The wavelength of wavenumber 1 is assumed to be the circumference of the earth at 67°S (15 640 km), almost corresponding to the circumpolar distance around the Antarctic continent. A representative depth profile around Antarctica is used by averaging the depth profiles in longitudes 0°–150°E and 160°–60°W to exclude Weddell and Ross Seas (Fig. 8a).

For simplicity, the wind stress is assumed to be parallel to the coast and constant in the cross-shore direction, neglecting the variation of wind stress in that direction and thus the wind stress curl. This is partly based on the fact that the wind stress near the coast is responsible for the sea level variations from our numerical experiments (Figs. 2b and 3) and that the spatial scale of the atmospheric variation is much larger than that of the shelf and slope. Further, Gill and Schumann (1974) showed that alongshore wind stress at the coast is the main element for the generation of shelf waves through the blocking effect of onshore Ekman flux. For the analytical solutions, realistic alongshore wind stress around Antarctica from 1994 to 1999, the same wind product for the space–time spectral analysis in section 3, was used to calculate the amplitude and phase of the forcing term in the frequency–wavenumber domain. In the following subsections, we discuss both wavenumber-zero and propagating modes in detail.

a. Wavenumber-zero ($k = 0$) mode

1) ANALYTICAL SOLUTION TO THE ALONGSHORE UNIFORM FORCING IN AN INFINITE DOMAIN

For barotropic, f-plane, linear, inviscid, and nondivergent motion, the shallow-water equations with a simple damping term have the form

$$\frac{\partial u}{\partial t} - fv = -g\frac{\partial \eta}{\partial x} - r_t u + \frac{X}{H}, \tag{1}$$

$$\frac{\partial v}{\partial t} + fu = -g\frac{\partial \eta}{\partial y} - r_t v, \tag{2}$$

$$0 = \frac{\partial}{\partial x}(Hu) + \frac{\partial}{\partial y}(Hv), \tag{3}$$

where u and v are the depth-averaged components of velocity in the x and y directions, respectively; η is the elevation of the sea surface above the equilibrium level; f is the Coriolis parameter at 67°S; $X = X(t)$ is the x component of wind stress acting on the ocean surface, divided by the density of the water; g is the acceleration of gravity; and dissipation is parameterized in proportion to the velocity with the damping time scale r_t^{-1}. Taking $r_t = r/H$, this dissipation would represent the spindown effect by bottom friction, as in the numerical model equations. We here simplify r_t to a constant value,

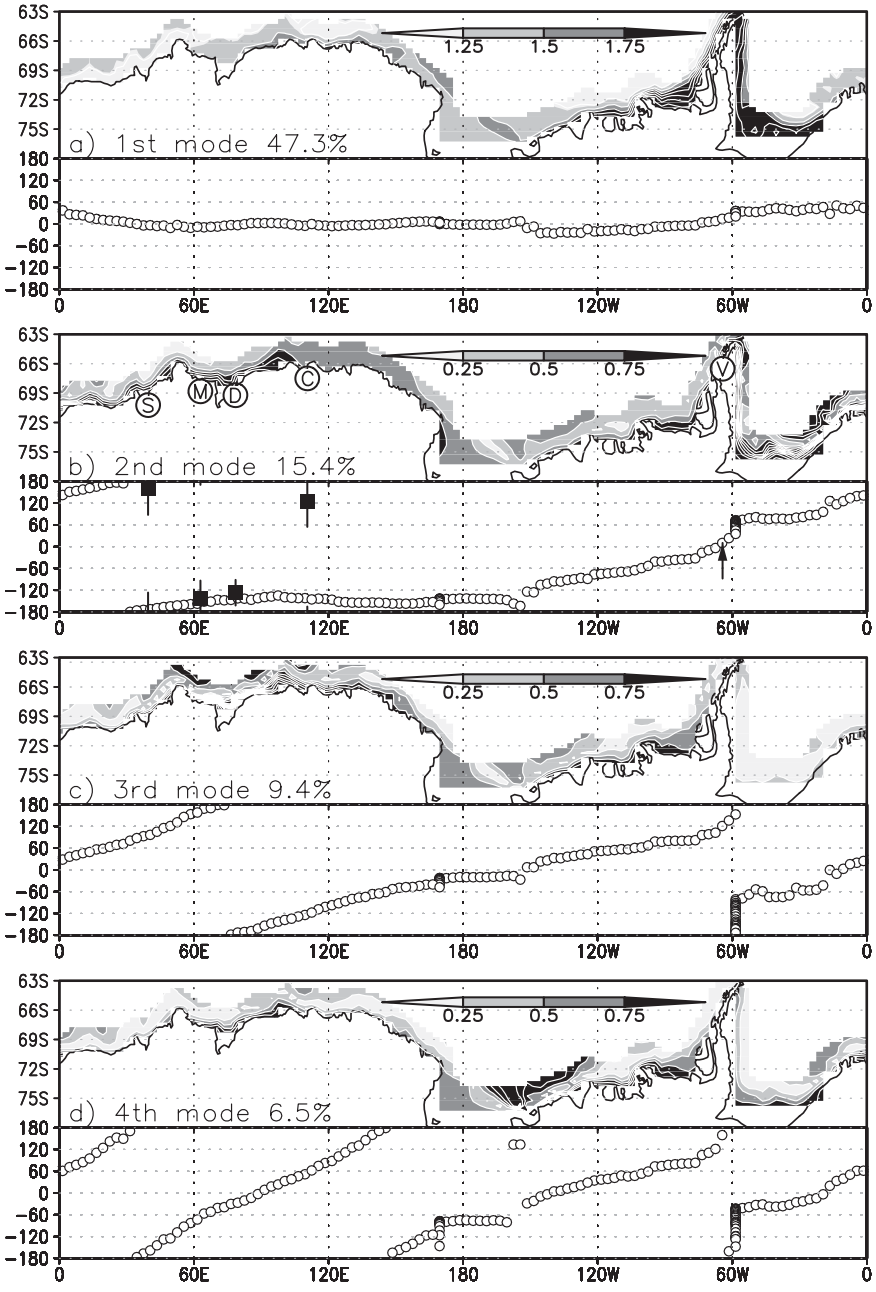

FIG. 7. Spatial distribution of the amplitude and phase at the coast around Antarctica from CEOF analysis of the sea level in the model: See the text for the specific procedure of the analysis. (a)–(d) The results of the first–fourth modes from CEOF analysis. The contribution of each mode is indicated at the middle in each panel. The phase at the nearest grid point from the coast is shown as a function of longitude. Propagation of the phase is in the direction of decreasing phase. In (b) the phase differences of four stations (Syowa, Mawson, Davis, Casey) with the Vernadsky Station (indicated by arrow) are shown as squares with 95% error bars.

following Wearn and Baker (1980) and Weijer and Gille (2005). For considering the uniform variation in the alongshore direction, we can neglect the term $\partial/\partial x$ in (1) and (3). From (3), the offshore mass flux, Hv, must have constant value. Additionally, from the coastal boundary condition ($Hv = 0$ at $y = 0$), v must vanish in the domain. From (1)–(3), we can obtain

$$\left(\frac{\partial}{\partial t} + r_t\right)\frac{d\eta}{dy} = -\frac{f}{gH}X. \tag{4}$$

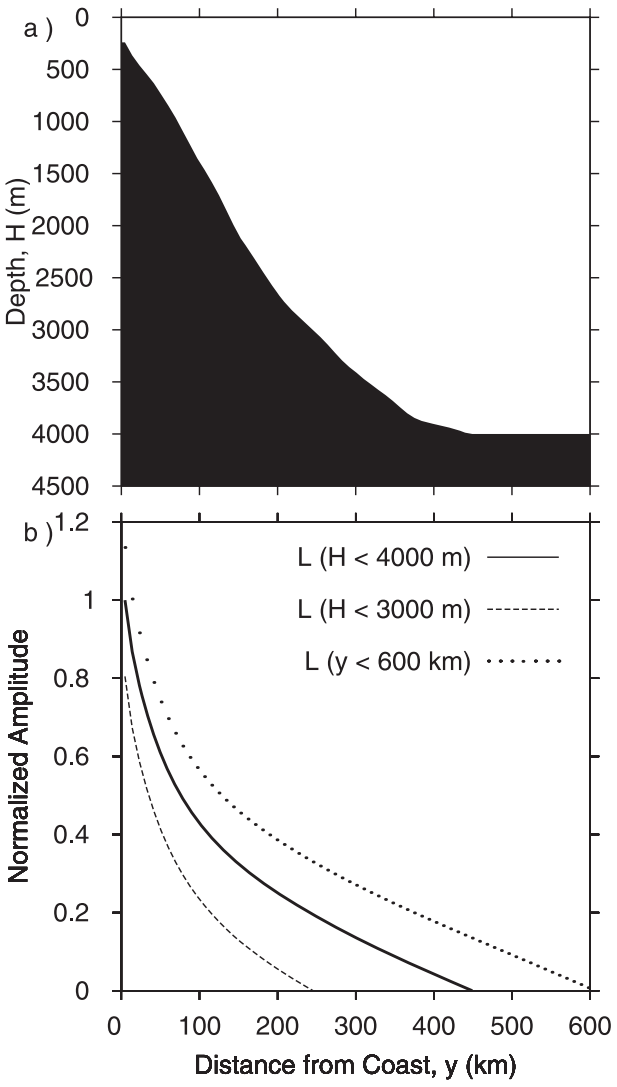

FIG. 8. (a) Bottom depth profile used in the solutions and (b) cross-shore structures of sea level for the wavenumber-zero solution. In (b) solid line shows the solution by the integration from the end of slope (baseline case), which is mainly used in this study. Dots and dashed lines show the solution by integration from 600 km and from the position where the depth is 3000 m, respectively. Amplitudes are normalized with the amplitude at the coast in the baseline case.

We consider the oceanic response to the sinusoidal forcing $X = X_0(\omega)\sin(\omega t + \theta)$, where X_0, ω, and θ are amplitude, frequency, and phase of wind stress, respectively. The solution of (4) becomes

$$\eta(y,t) = \eta(L,t) + \frac{f X_0}{g\sqrt{r_t^2 + \omega^2}} \int_L^y \frac{1}{H} dy \cos(\omega t + \theta + \delta), \tag{5}$$

where $\eta(L, t)$ is the sea level determined by integration of the forcing from infinity to $y = L$; $\delta(\tan\delta = r_t/\omega)$ is the phase difference from an inviscid solution. From the numerical experiments (Figs. 2b and 3), the offshore forcing in deep ocean was found to be a minor contributor to the coastal sea level. For simplicity, we assume $\eta(L, t) = 0$ in this study. The cross-shore structure depends on the position of the boundary, $y = L$ (Fig. 8b). The nondivergent approximation implicitly assumes that L is smaller than the external Rossby radius. Further, the sea level set up by the forcing in deep flat ocean is relatively small in the solution (5). All these considered, we set the position of L to the end of the slope hereafter, although we admit that the position of L is arbitrary. In any cases, the phase relation between the oceanic response and the forcing is the same.

The cross-shore structure in (5) can be decomposed as

$$\int_L^y \frac{1}{H} dy = \frac{1}{H_d}\left[(y - L) + \int_L^y \left(\frac{H_d}{H} - 1\right) dy\right],$$

where H_d is the maximum depth. The first and second terms in the brackets correspond to a component determined by the flat ocean dynamics and the component that is caused by the topographic gradient, respectively. The first term varies linearly toward the coast while the second term varies exponentially. It is considered that the trapping feature of the sea level over the shelf and slope (Fig. 6) comes from the second term. The first term creates the constant flow ($\propto H_d^{-1}$) with no vorticity. On the other hand, the second term creates the shear flow [$\propto H_d^{-1}(\frac{H_d}{H} - 1)$] with the vorticity ($\propto H^{-2} dH/dy$) over the shelf and slope. In the physical point of view, the second term results from the vorticity input due to vortex stretching/shrinking through the compensation flow of Ekman flux blocked at coastal boundary, causing the trapping feature for both the sea level and flow over the shelf and slope.

2) CHARACTERISTIC OF THE SOLUTION AND COMPARISON OF OBSERVATIONAL AND MODEL RESULTS

To focus on the coherent sea level variation, we compared the leading mode from EOF analysis in the observation with the analytical solutions for the wavenumber-zero mode. Although we only show the results of comparison between the observation and the solutions, similar or better results were obtained when the model results were used instead of the observation.

Five analytical solutions of the wavenumber-zero mode ($k = 0$) were calculated: a case with no damping term and four cases with a damping term with time scales (r_t^{-1}) of 50, 10, 5, and 1 days. Spectral analyses (power and cross-spectra) were performed for the observation and the five solutions for wavenumber zero to

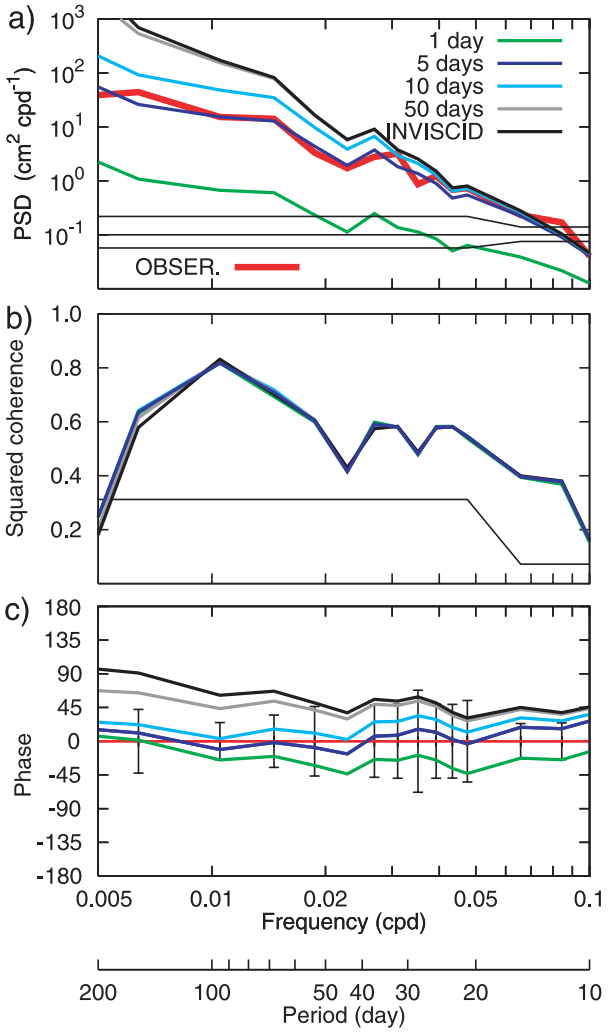

FIG. 9. (a) Power spectra of the observed sea level (the leading mode of EOF analysis) and the five analytical solutions, (b) squared coherence, and (c) phase of the cross-spectra between observation and solutions. In (c) a positive value indicates that the solution leads the observation. The 95% confidence interval levels are shown in (a) and (b). Confidence intervals for phase are calculated for the solution with a 5-day damping time scale, shown in (c) by vertical bars centered on zero.

compare them in the frequency domain. Figure 9 shows power spectra of the observation and the five solutions (Fig. 9a), squared coherences (Fig. 9b), and phase differences of cross spectra between the observation and solutions (Fig. 9c). The solution with a smaller damping term has larger amplitude than that observed (Fig. 9a) and also larger phase differences from the observation at lower frequencies (Fig. 9c). From the power spectra (Fig. 9a), the observed amplitude has a similar magnitude to that of the solution with a 5- or 10-day damping time scale at periods from 10 to 200 days with 95% confidence. Although the squared coherences between the observation and any solutions are similarly above the confidence level of 95% at almost all frequencies (Fig. 9b), the phase differences are significantly different among the solutions (Fig. 9c). The solution with a 5- or 10-day damping time scale coincides well with the observation in phase at periods from 10 to 200 days. Both in the amplitude and phase, the solution with a 5-day damping time scale is the best-fit solution to the observed coherent sea level variation. We adopt this solution for further comparison with the observed and modeled sea levels.

The time series of this solution with a 5-day damping time scale (blue in Fig. 5) is very similar to that of the observation (red in Fig. 5) and model (green in Fig. 5), where all three time series are constructed from the superposition of the components at periods from 10 to 200 days. The correlation coefficient between the solution and observation (model) is 0.77 (0.88). In spite of its simplicity, the solution can reproduce well the observed coherent sea level as well as the model result.

To examine the characteristics of the response of coastal sea level to the forcing in the frequency domain, the gain factor (Fig. 10a) and power spectrum (Fig. 10b) of the analytical solution with a 5- or 10-day damping time scale are calculated for each wavenumber. The gain factor is defined as the square root of the ratio of the power spectrum of the coastal sea level (Fig. 4b) and that of the wind stress (Fig. 4a). The gain factor and power spectrum for the wavenumber-zero solution with a 5-day damping time scale are shown by red lines in Fig. 10. For the wavenumber-zero mode ($k = 0$), the amplitude in (5) is proportional to

$$\frac{f}{g}\frac{1}{\sqrt{r_t^2 + \omega^2}}. \tag{6}$$

At high frequencies ($\omega \gg r_t$), this term is approximated by $(g^{-1}f)\omega^{-1}$ and thus varies inversely proportional to the frequency. At low frequencies ($\omega \ll r_t$), corresponding to periods longer than ~100 days, the term approaches a constant value of $(g^{-1}f)r_t^{-1}$, implying that the forcing term approximately balances the damping term. The gain factor of the wavenumber-zero coastal sea level in both the observation (crosses in Fig. 10a) and model (closed and open circles in Fig. 10a) shows a similar spectral feature to that in the wavenumber-zero solution. Correspondingly, the power spectrum of the solution with a 5-day damping time scale (red line in Fig. 10b) also shows similar features to those of coherent sea level in both the observation and model (Figs. 4b and 9a). It should be noted that the response dependency of the wavenumber-zero mode on the

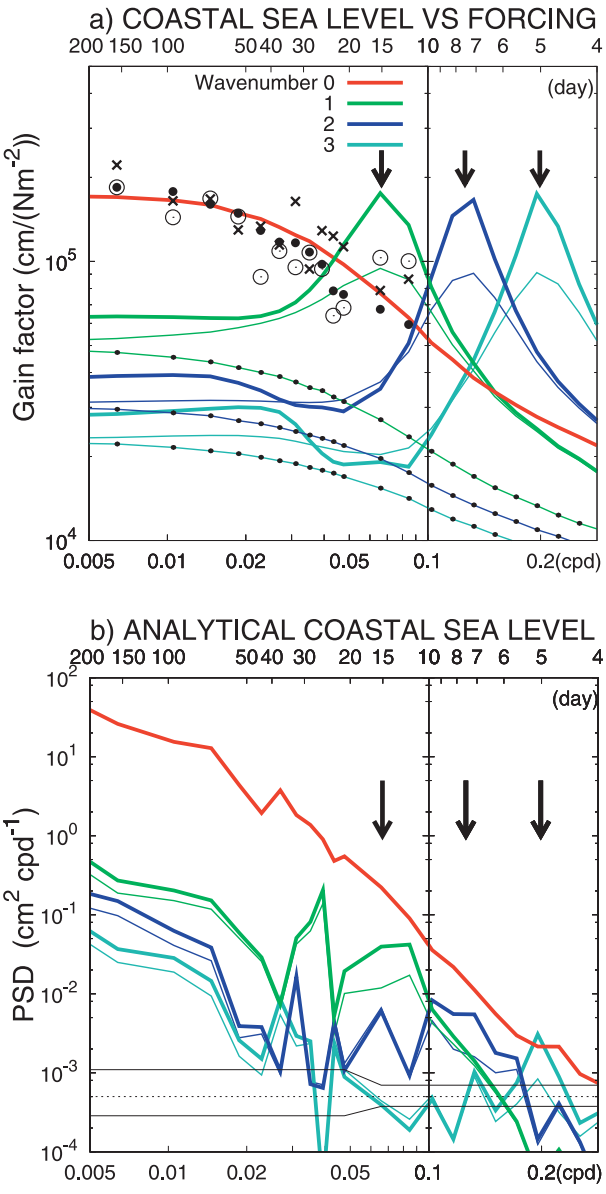

FIG. 10. (a) Gain factor and (b) power spectra of the coastal sea level in the analytical solution. In both panels the wavenumber-zero solution with a 5-day damping time scale is shown by red lines and the westward solutions for wavenumber 1–3 with 5- and 10-day damping time scale are indicated by thin and thick lines, respectively. In (a) lines with dots show the eastward components of the solution with a 5-day damping time scale. In (a) crosses and circles denote the gain factor with respect to the wavenumber-zero forcing for the observed coherent sea level (the leading mode of EOF analysis) and for the modeled one (closed circles: the leading mode of EOF analysis; open circles: wavenumber-zero component), respectively. In (b), since the power spectra of the eastward components are small, the power spectra of westward components are only shown to avoid mess in the figure. In (b) the band averaging is performed to the spectra of each wavenumber. In the horizontal axes of all panels, log and linear scales are used below and above 0.1 cpd, respectively. Arrows indicate the resonant periods derived from the analytical solution.

frequency [(6) and red line in Fig. 10a] can explain why the power spectrum of the wavenumber-zero sea level (Fig. 4b) at lower frequencies has a steeper dependence on frequency than that of the wavenumber-zero wind stress (Fig. 4a).

Since the AAO is by far a dominant atmospheric signal in the Southern Hemisphere, all of the wind stress in the coastal region, wind stress in the offshore area, wind stress curl, and sea level pressure have high correlation with the AAO index. Thus, the oceanic variations including sea level variations around Antarctica inevitably are affected by the AAO either directly or indirectly. Even if the sea level variations around Antarctica were determined by another factor (e.g., wind stress curl), the wind stress in the coastal region or the associated solution would have high correlation with the sea level because the coastal wind stress could inevitably be affected by the AAO.

Using a correlation analysis, we examined whether the wavenumber-zero solution can explain the observed coherent sea level variation around Antarctica better than the wind stress or the AAO variation itself can. Table 1 summarizes the correlation coefficients of the observed sea level (OBS), AAO index (AAO), and sea level that excludes the AAO component (OBS − AAO) with the wind stresses and analytical solutions. We used the wind stresses in the coastal region (CW) and the offshore region (DW, averaged over the latitudinal range of the Drake Passage, 54°–63°S). For the solution with a 5-day damping time scale, that forced by the CW was used (CS, blue in Fig. 5). For comparison, the solution forced by the DW with a 5-day damping time scale (DS) was also calculated. Time series with the AAO effect removed (indicated by X−AAO) are calculated as the original time series minus $b_{\mathrm{AAO}} \times$ AAO index, where b_{AAO} is the regression coefficient of the variable onto the AAO index. This time series of $b_{\mathrm{AAO}} \times$ AAO index is the component explained by the AAO variation in the original time series. The AAO index certainly has significant correlation with both wind stresses (CW and DW) and the associated solutions (CS and DS), as expected. A noticeable point in Table 1 is that the sea level component that is independent of the AAO (OBS−AAO) can be explained well only by the solution forced by the coastal wind stress (correlation coefficient: CS−AAO 0.64), although the original sea level (OBS) correlates with both the wind stresses and associated solutions. These analyses suggest that only the solution forced by the coastal wind stress can explain the observed coherent sea level variation and that such agreement is not just a result of the dominant influence of the AAO.

TABLE 1. Correlation coefficients of the observed coherent sea level (OBS, the leading mode of EOF analysis), AAO index (AAO), and sea level that excludes the AAO component (OBS − AAO) with the alongshore wind stresses and associated analytical solution: CW and DW indicate wind stresses averaged over the coastal region and the region between 54° and 63°S, respectively; CS and DS are the solution from "CW" and "DW" with a 5-day damping time scale, respectively. See the text for further explanations. Correlation coefficient for the 99% significance level is 0.06.

	−AAO	−CW	−DW	CS (5 day)	DS (5 day)
vs OBS	0.65	0.63	0.67	0.77	0.64
vs –AAO	(1.00)	0.57	0.83	0.56	0.69
	AAO	−(CW − AAO)	−(DW − AAO)	CS − AAO	DS − AAO
vs (OBS − AAO)	(0.00)	0.41	0.30	0.64	0.35

b. Westward propagating mode

1) ANALYTICAL SOLUTION OF BAROTROPIC SHELF WAVES IN CIRCUMPOLAR DOMAIN

The configurations of the analytical model for the barotropic shelf wave, including governing equations and coordinate system, are the same as those considered by Gill and Schumann (1974, see the detailed formulation therein) except for the cyclic boundary condition in zonal domain.

In reality, the coastal oceanic response is manifested by the coastally trapped waves that include the effects of stratification. As shown in the appendix, the coastally trapped waves of the Antarctic coastal ocean become nearly barotropic shelf waves owing to the weak stratification; therefore, the barotropic assumption is made. Since the alongshore scale is much larger than the cross-shore scale of the relevant sea level features, a long-wave approximation is used.

We considered the oceanic response to sinusoidal forcing: $X(x,\ t) = X_0 \sin(kx - \omega t + \theta)$. The phase ($\theta$) and amplitude ($X_0$) of the forcing can vary with both wavenumber (k) and frequency (ω). The streamfunction ψ for each cross-shore mode n can be expressed by the product of cross-shore variation $F_n(y)$ and the alongshore temporal variation $\phi_n(x,\ t)$. For the sinusoidal forcing, the alongshore-temporal variation term of an exact solution at $x = x_0$ and $t = t_0$ with a simple damping, which is the same representation as those considered by Gill and Schumann, is

$$\phi_n(x_0, t_0) = \frac{b_n X_0}{f} \frac{1}{(k - \omega/c_n)} \times \cos\delta \cos(kx_0 - \omega t_0 + \theta + \delta), \quad (7)$$

where c_n and b_n are the phase velocity of a free shelf wave and a coefficient to expand the forcing term for each cross-shore mode. The values of these coefficients for the depth profile of Fig. 8a are listed in Table 2. Negative values of c_n indicate that the waves propagate with the coast on the left, that is, westward.

The solution of (7) is a modified one from the inviscid solution, with a reduction of amplitude by

$$\cos\delta = \frac{(k - \omega/c_n)}{\sqrt{r_x^2 + (k - \omega/c_n)^2}}$$

and a phase difference of δ (where r_x is the coefficient of the damping spatial scale, associated with the damping time scale r_t through the equation $r_x = r_t/c_n$). For a certain wavenumber and frequency, the streamfunction is expressed by the superposition of cross-shore modes, and the sea level variation $\eta(x, y, t)$ can be obtained by integrating the geostrophic balance in the cross-shore direction:

$$\eta(x,\ y,\ t) = \eta(x,\ L,\ t) + \sum_n \phi_n(x,\ t) \int_L^y \frac{f}{gH(y')} \frac{dF_n(y')}{dy'} dy'. \quad (8)$$

The realistic sea level variation is calculated by the sum of components of all wavenumbers and frequencies.

2) CHARACTERISTICS OF SHELF WAVE MODES

For the propagating mode, the amplitude in (7) can be rewritten as

$$\frac{b_n X_0}{f} \frac{1}{\sqrt{r_x^2 + (k - \omega/c_n)^2}} = \frac{b_n X_0}{f} \frac{c_n c_f}{\sqrt{(c_f r_t)^2 + \omega^2 (c_n - c_f)^2}}, \quad (9)$$

TABLE 2. Values of c_n and b_n for the first five modes of the shelf wave. Negative values of c_n indicate westward propagation.

	n				
	1	2	3	4	5
c_n (m s^{-1})	−12.02	−3.91	−1.72	−0.93	−0.62
$b_n \times 10^2$	3.36	2.96	2.44	2.14	1.90

where $c_f = \omega/k$ is a phase velocity of the wind stress. Resonance would occur when the phase velocity of the wind stress (c_f) approaches that of the shelf waves (c_n), which has a westward propagating direction. Thus, the resonance is only possible for the case of westward propagating forcing.

In this subsection, we examined the characteristics of the resonance of the westward propagating mode. From the phase velocity of the first shelf wave mode (Table 2), the resonant periods of the westward propagation at wavenumbers 1, 2, and 3 are 15, 7.5, and 5 days, respectively. We adopt the damping time scale of 5 and 10 days for further analyses, assuming that it is similar to that of the wavenumber-zero mode. Damping time scale does not affect the resonant period, but changes the amplitude (9).

Because of these characteristics of resonance, the gain factor of the analytical solution for $k = -1, -2, -3$, derived from the superposition of cross-shore modes of the shelf wave, shows a peak at the resonant frequency of the first shelf wave mode (arrows in Fig. 10a). Since the value of $c_n b_n$ of the higher shelf wave modes ($n \geq 2$) is much smaller than that of the first shelf wave mode (Table 2) and the cross-shore amplitude of the first shelf wave mode becomes largest at the coast, only the resonance of the first shelf wave mode appears significantly. Figure 10b shows the power spectra of the solution for the purely propagating forcing (excluding components of the standing wave). In accordance with the gain factor (Fig. 10a), the power spectra of the solution show spectral peaks around the resonant frequencies for $k = -1, -2, -3$.

We compare the spectra of the solution with those of the modeled sea level (Fig. 4b). For comparison, we use the spectra of the solution for the purely propagating forcing (Fig. 10b) by excluding the standing wave components in the forcing. If the geometry were an idealized one, that is, the Antarctic coastline exactly followed the latitudinal line and water depth were uniform in the alongshore direction, we should use the solution for the full forcing including the standing wave forcing. Since the spatial structure of the AAO is almost annular in the Antarctic Ocean and the inherent atmospheric standing wave is small, most part of standing wave in the atmospheric forcing in the circumpolar coastal grid arises from the variation of coastline. Also, for the ocean under the realistic topography, the component of the standing waves in circumpolar coastal grid probably comes from the irregular coastline and variable water depth in the alongshore direction. For these reasons, the solution for the purely propagating forcing should be used for the comparison. The power spectra of the solution for the purely propagating forcing with a 10-day damping time scale (Fig. 10b) show similar profiles to those of the modeled sea level (Fig. 4b). These suggest that the solution with a 10-day damping time scale can roughly explain the westward propagating mode.

Next, we examined whether the westward propagating signals, suggested by the analytical solution, can be identified in the real ocean. We tried to identify the westward propagating signals at wavenumber 1 in the observations as follows. First, a bandpass filter was applied to the observed sea level variations to extract signals at periods from 3 to 20 days. Second, the component of the coherent mode was estimated by EOF analysis and removed from the original bandpassed sea level variation. A coherent mode appears as the first mode of EOF analysis in this frequency range. Third, from the residual signals, the squared coherences and phase differences of the cross-spectra averaged over periods from 13 to 16 days, around the resonant period for wavenumber 1, were calculated. Since only the Vernadsky Station is far away from the other four stations, the phase differences of the four stations to the Vernadsky Station were used to identify the westward propagating signals at wavenumber 1. Since the second mode of the CEOF analysis for the model result (Fig. 7b) corresponds to the westward propagating mode at wavenumber 1, the relative phase differences of the four stations to the Vernadsky Station are superimposed in Fig. 7b. It is found that the phase differences in the observation roughly coincide with those in the model result. The squared coherences at all four stations with the Vernadsky Station are statistically significant above 95%. These are consistent with the existence of the westward propagating mode at wavenumber 1 in the real ocean. Given the fact that the observational stations are very scarce around Antarctica at present, it is difficult to discuss the propagation phenomena, including the existence of the higher modes ($k \leq -2$), in more detail. In the future, spatially denser observations around Antarctica will hopefully enable us to detect these westward propagating signals.

5. Summary and discussion

Using a barotropic shallow-water model, we investigated the dynamics of sea level variation around Antarctica. The barotropic numerical model, incorporating realistic wind stress and bottom topography, reproduces well the observed sea level variations around Antarctica (Fig. 2) as was presented by the previous studies (Vivier et al. 2005). These coastal variabilities are found to be trapped over the shelf and slope (Figs. 6 and 7). As a mechanism of these trapped signals, we consider analytical solutions of oceanic response to the alongshore

wind stress over the shelf and slope in the circumpolar domain. The coherent sea level variation at periods from 10 to 200 days can be explained by the wavenumber-zero solution (5) with a 5- or 10-day damping time scale (Fig. 9).

This wavenumber-zero solution has the same frequency dependence as that of Wearn and Baker (1980), which discussed the ACC response to the circumpolar-averaged wind stress in a flat ocean. However, the trapping feature over the shelf and slope, which characterizes the coherent variation, comes from the vorticity input due to vortex stretching/shrinking through the compensation flow of Ekman flux blocked at coastal boundary. Therefore, the existence of wind stress at the coastal boundary is crucial for the generation of the variation. Both numerical experiments (2b and 3) and correlation analysis (Table 1) also demonstrated that the coherent variation around Antarctica is mainly driven by the wind stress at the coastal boundary and not by the offshore wind stress.

For the damping mechanisms of the analytical solution, we implicitly parameterized the spindown by the bottom friction, topographic form drag, scattering damping of coastal geometry, and so on. Assuming that the damping is caused by bottom friction with coefficient $r = 5.0 \times 10^{-4}$ m s^{-1} (Chapman et al. 1986), the time scale of spindown for typical coastal shelf depths around Antarctica, taking $H = 500$ m (Fig. 8a), is estimated to be ~12 days. This damping time scale for shallow region is within the same order of that of the best-fit solutions. As in the case of the ACC variation (Weijer and Gille 2005), topographic form drag can be also a candidate for the dissipative mechanism even for the flow over the shelf and slope. More specific dissipation mechanism remains in the future.

In addition to the coherent mode, we identified westward propagating signals in the model that have wavenumbers 1, 2, and 3 in the zonal domain (Fig. 4b). These signals were also trapped over the shelf and slope (Fig. 7). Resonance of the shelf waves in the analytical solution can explain the spectral peaks at 15-, 7.5-, and 5-day periods (Figs. 4b and 10a,b). The phase relation of observed sea level at periods from 13 to 16 days is consistent with the existence of the westward propagation mode at wavenumber 1 in the real ocean (Fig. 7b).

Why is the coherent sea level variation by far the dominant feature? In general, around Antarctica the atmospheric synoptic-scale disturbances tend to propagate eastward, as shown in Fig. 4a. The westward propagating shelf wave modes in the Antarctic coastal region hardly respond to the eastward propagating forcing. In contrast, the wavenumber-zero mode solution can respond to the wavenumber-zero forcing at any frequency and the degree of the response increases with decreasing frequency [(6) and Fig. 10a]. In addition, the wavenumber-zero wind stress corresponding to the AAO variation is by far dominant forcing (Fig. 4a). Therefore, the coherent sea level variation around Antarctica is predominantly generated, particularly at lower frequencies (Figs. 4b and 10a,b).

For current variations over the shelf and slope, the coherent mode can be a dominant component as well as for sea level variations. In the model and analytical solution, the current and volume transport variations over the shelf and slope can reach values of ~10 cm s^{-1} and ~5 Sv (Sv $\equiv 10^6$ m^3 s^{-1}), respectively. The relation between the coherent mode and the currents over the shelf and slope around Antarctica seems to be an interesting topic of research for future studies.

Acknowledgments. We are much indebted to Drs. M. Wakatsuchi, A. Kubokawa, F. Mitsudera, S. Aoki, G. Mizuta, and N. Hirose for their instructive comments, and deeply thank Y. Fukamachi for his critical reading of the manuscript. We thank K. H. Brink and D. C. Chapman for a Fortran program ''BIGLOAD2'' for calculation of coastally trapped waves. We appreciate editor Dr. E. Firing for his crucial comments on the analytical solutions, and are grateful to two anonymous reviewers for helpful comments on the manuscript. Numerical calculations were performed on the Pan-Okhotsk Information System of ILTS. K. K. is supported by the 21st Century Center of Excellence Program funded by MEXT (Ministry of Education, Culture, Sports, Science and Technology) and Core Research for Evolutional Science and Technology funded by Japan Science and Technology Agency.

APPENDIX

Validity for Barotropic and Long-Wave Approximations

In a realistic ocean that includes stratification, the coastal ocean response is involved with coastally trapped waves that have hybrid properties of barotropic shelf waves and internal Kelvin waves. To examine the validity of the barotropic and long-wave approximations, an exact solution of the coastally trapped waves for the Antarctic coastal ocean was calculated using the program ''BIGLOAD2'' (Brink 1982; Brink and Chapman 1987). A representative stratification in the Antarctic Ocean (Fig. A1a) was derived from the *World Ocean Atlas* 2001 dataset (Conkright et al. 2002). The phase velocities of the barotropic shelf waves under long-wave approximation are almost identical to those of the coastally trapped waves at least up to

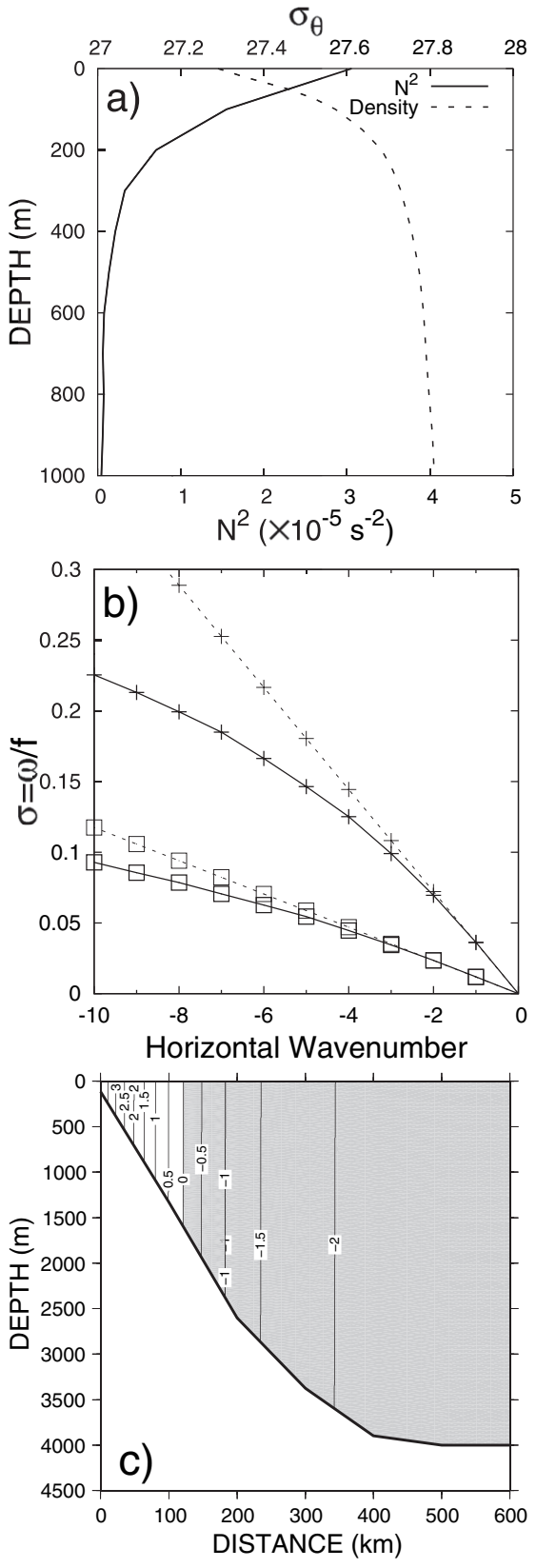

wavenumber 3 (Fig. A1b). A cross-shore structure for the first mode at wavenumber 1 (Fig. A1c) clearly illustrates that the wave has near barotropic structure. The second and third modes of coastally trapped waves also exhibit near barotropic structure (not shown). These calculations confirm the validity of the barotropic and long-wave approximations.

REFERENCES

Aoki, S., 2002: Coherent sea level response to the Antarctic Oscillation. *Geophys. Res. Lett.,* **29,** 1950, doi:10.1029/2002GL015733.

Barnett, T. P., 1983: Interaction of the monsoon and Pacific trade wind system at interannual time scales. Part I: The equatorial zone. *Mon. Wea. Rev.,* **111,** 756–773.

Brink, K. H., 1982: A comparison of long coastal trapped wave theory with observations off Peru. *J. Phys. Oceanogr.,* **12,** 897–913.

——, and D. C. Chapman, 1987: Programs for computing properties of coastal trapped waves and wind-drive motions over the continental shelf and slope. Woods Hole Oceanographic Institution Tech. Rep. WHOI-87-24, 2nd ed. 119 pp.

Chao, Y., and L.-L. Fu, 1995: A comparison between the TOPEX/POSEIDON data and a global ocean general circulation model during 1992–1993. *J. Geophys. Res.,* **100,** 24 965–24 976.

Chapman, D. C., J. A. Barth, and R. C. Beardsley, 1986: On the continuity of mean flow between the Scotian Shelf and the Middle Atlantic Bight. *J. Phys. Oceanogr.,* **16,** 758–772.

Conkright, M. E., R. Locarnini, H. E. Garcia, T. D. O'Brien, T. P. Boyer, C. Stephens, and J. I. Antonov, 2002: World Ocean Atlas 2001: Objective analyses, data statistics, and figures, CD-ROM documentation. National Oceanographic Data Center Internal Rep. 17, 17 pp.

Csanady, G. T., 1982: *Circulation in the Coastal Ocean.* Reidel, 279 pp.

Fahrbach, E., G. Rohardt, and G. Krause, 1992: The Antarctic Coastal Current in the southeastern Weddell Sea. *Polar Biol.,* **12,** 171–182.

Fu, L.-L., and R. A. Davidson, 1995: A note on the barotropic response of sea level to time-dependent wind forcing. *J. Geophys. Res.,* **100,** 24 955–24 963.

Gill, A. E., and E. H. Schumann, 1974: The generation of long shelf waves by the wind. *J. Phys. Oceanogr.,* **4,** 83–90.

Gille, S. T., D. P. Stevens, R. T. Tokmakian, and K. J. Heywood, 2001: Antarctic Circumpolar Current response to zonally averaged winds. *J. Geophys. Res.,* **106,** 2743–2759.

Hall, A., and M. Visbeck, 2002: Synchronous variability in the Southern Hemisphere atmosphere, sea ice, and ocean resulting from the annular mode. *J. Climate,* **15,** 3043–3057.

←

FIG. A1. (a) Vertical profile of potential density (dashed line) and buoyancy frequency N^2 (solid line) used in the coastally trapped wave calculation. (b) Dispersion relations for the first (crosses) and second (squares) modes of coastally trapped waves (solid lines) and of barotropic shelf waves (dashed lines) from the long-wave approximation: A negative wavenumber indicates westward propagation. (c) Cross-shore modal structure for pressure of the first mode coastally trapped wave for wavenumber 1: Amplitudes of the modal structure are arbitrary.

Hayashi, Y., 1971: A generalized method of resolving disturbances into progressive and retrogressive waves by space Fourier and time cross-spectral analyses. *J. Meteor. Soc. Japan,* **49,** 125–128.

Hirose, N., I. Fukumori, and R. M. Ponte, 2001: A non-isostatic global sea level response to barometric pressure near 5 days. *Geophys. Res. Lett.,* **28,** 2441–2444.

Horel, J. D., 1984: Complex principal component analysis: Theory and examples. *J. Climate Appl. Meteor.,* **23,** 1660–1673.

Hughes, C. W., M. P. Meredith, and K. J. Heywood, 1999: Wind-driven transport fluctuations through Drake Passage: A southern mode. *J. Phys. Oceanogr.,* **29,** 1971–1992.

——, P. L. Woodworth, M. P. Meredith, V. Stepanov, T. Whitworth, and A. R. Payne, 2003: Coherence of Antarctic sea levels, Southern Hemisphere Annular Mode, and flow through Drake Passage. *Geophys. Res. Lett.,* **30,** 1464, doi:10.1029/2003GL017240.

Meredith, M. P., and C. W. Hughes, 2004: On the wind-forcing of bottom pressure variability at Amsterdam and Kerguelen islands, southern Indian Ocean. *J. Geophys. Res.,* **109,** C03012, doi:10.1029/2003JC002060.

——, J. M. Vassie, K. J. Heywood, and R. Spencer, 1996: On the temporal variability of the transport through Drake Passage. *J. Geophys. Res.,* **101,** 22 485–22 494.

——, P. L. Woodworth, C. W. Hughes, and V. Stepanov, 2004: Changes in the ocean transport through Drake Passage during the 1980s and 1990s, forced by changes in the Southern Annular Mode. *Geophys. Res. Lett.,* **31,** L21305, doi:10.1029/2004GL021169.

Middleton, J. H., T. D. Foster, and A. Foldvik, 1982: Low-frequency currents and continental shelf waves in the Southern Weddell Sea. *J. Phys. Oceanogr.,* **12,** 618–634.

National Geophysical Data Center, 1988: Digital relief of the surface of the Earth. Data Announcement 88-MGG-02, NOAA, National Geophysical Data Center.

Ohshima, K. I., T. Kawamura, T. Takizawa, S. Ushio, and T. Miyakawa, 2000: Current variability under landfast sea ice in Lützow-Holm Bay, Antarctica. *J. Geophys. Res.,* **105,** 17 121–17 132.

Overland, J. E., and R. W. Preisendorfer, 1982: A significance test for principal components applied to a cyclone climatology. *Mon. Wea. Rev.,* **110,** 1–4.

Peterson, R. G., 1988: On the transport of the Antarctic Circumpolar Current through Drake Passage and its relation to wind. *J. Geophys. Res.,* **93,** 13 993–14 004.

Ponte, R. M., 1993: Variability in a homogeneous global ocean forced by barometric pressure. *Dyn. Atmos. Oceans,* **18,** 209–234.

——, and N. Hirose, 2004: Propagating bottom pressure signals around Antarctica at 1–2-day periods and implications for ocean modes. *J. Phys. Oceanogr.,* **34,** 284–292.

Thompson, D. W. J., and J. M. Wallace, 2000: Annular modes in the extratropical circulation. Part I: Month-to-month variability. *J. Climate,* **13,** 1000–1016.

Trenberth, K. E., W. G. Large, and J. G. Olson, 1990: The mean annual cycle in global ocean wind stress. *J. Phys. Oceanogr.,* **20,** 1742–1760.

Vivier, F., K. A. Kelly, and M. Harismendy, 2005: Causes of large-scale sea level variations in the Southern Ocean: Analyses of sea level and a barotropic model. *J. Geophys. Res.,* **110,** C09014, doi:10.1029/2004JC002773.

Wearn, R. B., and D. J. Baker, 1980: Bottom pressure measurements across the Antarctic Circumpolar Current and their relation to the wind. *Deep-Sea Res.,* **27A,** 875–888.

Weijer, W., and S. T. Gille, 2005: Adjustment of the Southern Ocean to wind forcing on synoptic time scales. *J. Phys. Oceanogr.,* **35,** 2076–2089.

Woodworth, P. L., J. M. Vassie, C. W. Hughes, and M. P. Meredith, 1996: A test of the ability of TOPEX/POSEIDON to monitor flows through the Drake Passage. *J. Geophys. Res.,* **101,** 11 935–11 947.

——, and Coauthors, 2006: Antarctic Peninsula sea levels: A real-time system for monitoring Drake Passage transport. *Antarct. Sci.,* **18,** 429–436.